applied sciences

MDPI

Article

Multi-Timescale Coordinated Optimization of an Integrated Electricity–Hydrogen–Ammonia Production System with Hybrid Hydrogen-Electricity Energy Storage

Zhengjian Chen [1], Shihao Zhu [2,3,*], Fulin Fan [2,3], Jingran Zhang [1], Jiang Qin [4,*] and Kai Song [2,3,*]

[1] Shenzhen Energy Group Company Ltd., Shenzhen 518033, China; chenzhengjian@sec.com.cn (Z.C.); zhangjingran@sec.com.cn (J.Z.)
[2] School of Electrical Engineering and Automation, Harbin Institute of Technology, Harbin 150001, China; fulin.fan@hit.edu.cn
[3] Suzhou Research Institute, Harbin Institute of Technology, Suzhou 215104, China
[4] School of Energy Science and Engineering, Harbin Institute of Technology, Harbin 150001, China
* Correspondence: 25b906043@stu.hit.edu.cn (S.Z.); qinjiang@hit.edu.cn (J.Q.); kaisong@hit.edu.cn (K.S.)

Abstract

Driven by global net-zero goals, the integrated electricity–hydrogen–ammonia system provides a pathway for coordinating renewable energy utilization with green chemical production. To address dynamic mismatch and control heterogeneity between electrical and chemical units, this paper presents a coupled multi-energy model and a multi-timescale scheduling strategy. First, nonlinear electrolyzer conversion, part-load ammonia auxiliary consumption and equipment degradation costs are incorporated into the hydrogen–electricity hybrid storage model. Then, a two-stage optimization architecture is designed: day-ahead mixed-integer programming for unit commitment, and intra-day CNN-LSTM dynamic rolling optimization. Finally, grid-connected and off-grid tests using normalized public load and photovoltaic profiles examine the coordinated operation of the system. Results show that all four grid-connected cases meet the daily ammonia delivery requirement of 200 kg, with operating margins ranging from −491.84 to 859.68 CNY/day. The three four-hour off-grid cases maintain ammonia production without load shedding under the tested conditions. These findings provide an operational reference for integrating renewable energy with green ammonia synthesis.

Keywords: hydrogen energy; ammonia synthesis; hybrid energy storage; multi-timescale optimization

Check for updates

Academic Editor: José A. Orosa García

Received: 23 October 2026
Revised: 16 November 2026
Accepted: 17 November 2026
Published: 24 November 2026

Copyright: © 2026 by the authors. Licensee MDPI, Basel, Switzerland. This article is an open access article distributed under the terms and conditions of the Creative Commons Attribution (CC BY) license.

1. Introduction

Under the momentum of global net-zero pathways, the green transition of the traditional fossil energy industry has become a critical priority for sustainable development. The Integrated Energy System (IES), which utilizes renewable energy for power generation, electrochemical energy storage, hydrogen storage, and other means to achieve the conversion and utilization of multiple energy forms while reducing fossil fuel consumption, serves as a key approach for decarbonizing the energy system [1,2]. In existing IES configurations, while hydrogen is advantageous for long-duration storage, its direct application is often constrained by the low round-trip efficiency of conversion processes and the substantial infrastructure costs associated with compression or liquefaction. Utilizing green hydrogen for ammonia synthesis can effectively address this issue [3,4].

Driven by the global imperative for deep decarbonization and the transition toward sustainable energy systems, Integrated Energy Systems (IES) have demonstrated significant potential in synergizing multiple energy carriers [5]. Current research has extensively explored the coordinated dispatch of electricity, heat, and gas. For instance, Wang et al. [6] deeply incorporated carbon flow regulation into the coordinated dispatch of multi-energy flows, proposing two modeling methods: "setting gas with heat" and "setting energy with carbon." These approaches realize a deep coupling of electricity, heat, gas, and carbon flows. By establishing a model based on the "setting energy with carbon" method—specifically, an integrated operational framework combining power-to-gas, carbon capture systems, and hydrogen fuel cells—they achieved dynamic optimization of "carbon-energy coordination." This effectively resolves the challenge of balancing emission reduction with economic benefits in IES. Liu et al. [7] addressed the multi-energy coordination challenges in multi-energy complementary integrated energy systems (MCIES) by introducing a flexibility index as the core optimization objective. They established a quantitative correlation model linking real-time dispatch of MCIES with carbon emission reduction—a methodology applicable to typical scenarios such as industrial parks and building clusters. In contrast, Li et al. [8] tackled the uncertainties in forecasting and the coupling characteristics of multiple energy flows in integrated energy systems. They developed a coordinated dispatch framework incorporating demand-side management, characterized by an architecture that integrates source-load interaction with dynamic correction. This provides both theoretical support and practical paradigms for the economical and low-carbon operation of regional energy systems with high penetration of renewable energy. Zhang et al. [9] constructed a systematic framework integrating mathematical modeling, algorithm design, and empirical verification to facilitate the standardized modeling of energy units such as water electrolyzers. They developed a multi-energy flow coordinated scheduling theoretical framework that accounts for full-duplex characteristics, providing a theoretical foundation for the optimal operation of distributed energy aggregators in future energy internet. Despite these advancements in power-side regulation, existing studies often simplify electrolyzers and other Power-to-X units into linear efficiency models. This simplification overlooks the complex electrochemical characteristics within these units, as well as the strict start-stop constraints and minimum load requirements of downstream chemical units, such as ammonia synthesis plants.

To address the economic challenges of long-term hydrogen storage and expand pathways for renewable energy integration, the production of green ammonia using green hydrogen has emerged as a significant technological direction. Utilizing hydrogen as an intermediate medium, the synthesis, storage, and utilization of ammonia facilitate long-term energy storage at a lower cost [10–12]. Regarding green hydrogen-based ammonia production, Pagani et al. [13] demonstrated through empirical analysis in the Netherlands that a 2.3 GW-scale green hydrogen system can achieve full decarbonization across the entire ammonia production process. Furthermore, optimizing the capacity ratio between electrolyzers and offshore wind power can reduce the levelized cost of hydrogen by approximately 12%. These research findings have been applied in the planning of the North Sea Hydrogen Corridor in the Netherlands, serving as a practical reference for the European Union's hydrogen strategy. Meanwhile, Armijo et al. [14] employed multi-time scale modeling to reveal the "flexibility premium" offered by wind–solar complementarity to integrated hydrogen–ammonia production systems. Their empirical data, reporting a green hydrogen cost of USD 2/kg, provided critical techno-economic evidence for the development of hydrogen corridors in South America, and has been cited by the International Energy Agency as a significant reference case for the commercialization of green hydrogen in developing countries. Müller et al. [15], through a full-life cycle energy efficiency matrix analysis, established the applicability boundaries of hydrogen–ammonia under different

storage duration scenarios, providing a quantitative theoretical basis for the selection of chemical energy storage technologies in the global energy transition. Although previous studies have explored the applications and economics of hydrogen and ammonia, they fail to construct a fully integrated electricity–hydrogen–ammonia energy chain, thereby limiting in-depth research on system-wide interactions. In terms of operational control, balancing day-ahead unit commitment with intraday real-time fluctuations remains a formidable challenge [16,17]. To address the multi-scale challenges arising from energy heterogeneity, Shen et al. [18] employed a model predictive control framework to implement rolling optimization scheduling for variables across fast and slow time scales, effectively managing the multiple uncertainties associated with electricity prices, renewable energy, and loads. Similarly, addressing the issue of seasonal imbalances in high-penetration renewable energy systems, Yang et al. [19] utilized a power curve characterization method based on a dual-feature ordered clustering network to accurately depict the seasonal evolution of supply and demand. This approach, combined with a multi-period variable-load start-stop strategy for electrolyzers, enhanced the regulation resilience of the system. Furthermore, Ma et al. [20] adopted a real-time transient energy analysis model to achieve dynamic performance evaluation spanning from components to the integrated system across scales. By integrating the 3E/3S indicator system, they also accomplished the collaborative optimization of capacity configuration. However, existing multi-energy complementary systems often confront a trade-off between algorithmic accuracy and response speed when coordinating hybrid energy storage with chemical production. Current optimization strategies still struggle to simultaneously reconcile day-ahead unit commitment with minute-level intra-day dynamic responses. Particularly under high renewable energy penetration, traditional deterministic optimization methods are inadequate for capturing the multi-variable and unpredictable dynamics inherent in 'Source-Load-Storage' interactions. Consequently, scheduling schemes often deviate from the optimal energy efficiency range during actual operation.

In the day-ahead electricity market, participants buy and sell electricity for delivery during specific time intervals of the following day. Prices are generally determined through auctions that match supply offers with demand bids, allowing producers and consumers to plan generation, consumption and expenditure in advance [21]. Within the proposed framework, day-ahead scheduling defines the hourly operating plan, whereas the case study adopts a historical time-of-use purchase tariff as its electricity–price input.

In summary, despite progress in multi-energy dispatch and hydrogen-based ammonia synthesis, current systems suffer from three fundamental flaws: efficiency drops when components operate dynamically, poor synchronization between short- and long-term storage, and fragile optimization models that fail under uncertainty. To address these challenges, this paper proposes a multi-stage collaborative optimization strategy. First, an electricity–hydrogen–ammonia multi-energy flow coupling model is constructed to elucidate the energy and material interaction mechanisms among electrolyzers, hydrogen storage tanks (HST), and ammonia synthesis units, specifically quantifying their interdependent energy-efficiency characteristics. Subsequently, a two-stage "day-ahead and intraday" optimization framework is designed. In the day-ahead stage, mixed-integer programming is employed to formulate unit commitment aimed at minimizing operational costs and grid dependency. In the intraday stage, a CNN-LSTM fusion framework is adopted to enable rolling prediction and dynamic power adjustment. Ultimately, a multi-timescale collaborative optimization scheme is derived to ensure the high-efficiency and stable operation of the green ammonia system under fluctuating renewable energy. The main contributions of the research are as follows:

(1) A mechanism-driven, high-fidelity dynamic model for the electricity–hydrogen–ammonia system is proposed. Abandoning the flawed fixed-coefficient and simplified

linear assumptions of past research, this model precisely captures the nonlinear efficiency shifts and dynamic behaviors of electrolyzers and ammonia units under realistically fluctuating conditions.

(2) A hierarchical "day-ahead and intra-day" optimization framework is designed to bridge the severe timescale gap. To resolve the clash between rapid renewable energy fluctuations (minute-level) and the sluggish inertia of ammonia synthesis (hour-level), this strategy assigns high-inertia start-stop decisions to day-ahead scheduling. Meanwhile, it uses intra-day rolling optimization for fast power balancing, seamlessly syncing electrical flexibility with chemical stability.

2. Description of the Proposed System

A single energy storage system cannot simultaneously meet both long-term and short-term energy storage demands. Therefore, integrating a hybrid hydrogen–electricity energy storage system (HESS) into renewable energy power generation has become a common approach. However, hydrogen storage currently faces challenges such as high costs and difficulties in long-distance transportation. Converting green hydrogen into green ammonia effectively addresses these issues. Thus, it is essential to design an Integrated Electricity–Hydrogen–Ammonia Production System architecture with HESS.

2.1. Design of an Integrated Electricity–Hydrogen–Ammonia Production System with HESS

As shown in Figure 1, the system is connected to the main grid via a DC microgrid and comprises a PEM water electrolyzer (PEMWE), an HST, an ammonia synthesis unit, and a battery. Within this system, the PEMWE and the battery absorb surplus renewable energy generation, converting it into hydrogen and electrical energy. Specifically, the PEMWE converts electricity into hydrogen, which is then transported via pipelines to the HST for subsequent supply as feedstock to the ammonia synthesis unit.

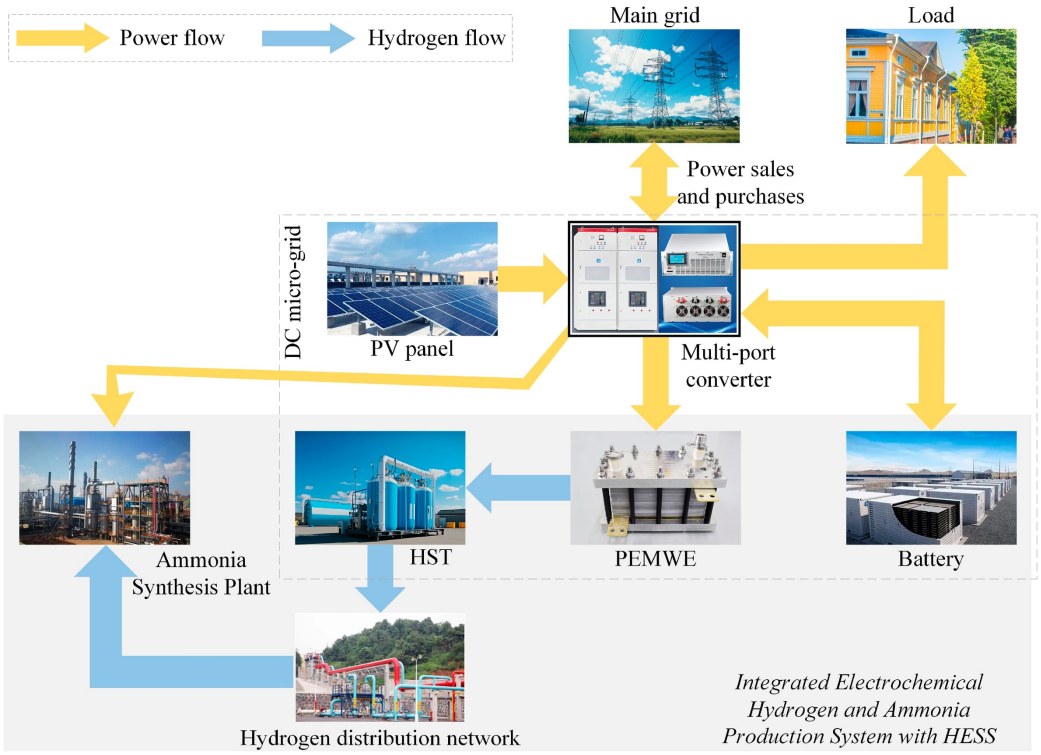


Figure 1. Design of an integrated electrochemical hydrogen and ammonia production system with an HES.

The core of this integration lies in the efficiency interdependence between the upstream water electrolysis and the downstream ammonia synthesis. If the PEMWE and the ammonia synthesis unit were directly connected, the inherent volatility of renewable energy would be transmitted through the hydrogen flow directly to the downstream process. However, the technical characteristics of the Haber–Bosch unit render it incapable of responding to such fluctuations. Consequently, the fluctuating hydrogen supply from the PEMWE directly dictates the operating point of the Haber–Bosch unit, creating a complex energy–efficiency correlation that transcends simple mass balance. To mitigate this, the HST is employed to isolate the two stages, acting as a critical buffer to facilitate the organic integration of these energy conversion devices.

In this configuration, both electrical and hydrogen energy forms coexist: electrochemical storage (battery) primarily responds to short-term, rapid load fluctuations, while hydrogen storage (HST) serves long-duration energy supply and stable raw material provision. As this study focuses on the multi-timescale coordination among electricity–hydrogen–ammonia components, power-to-hydrogen conversion devices (e.g., fuel cells) are not included in the baseline design. Furthermore, the system supports bi-directional power flow with the main grid to balance supply and demand. The following section details the modeling of each component within the system. Within the modeled boundary, hydrogen is used only as ammonia feedstock. The case study enables grid purchases and disables exports, while retaining the bidirectional hardware interface. Ammonia auxiliary electricity is supplied through the common electrical system.

2.2. Modeling of System

2.2.1. PEMWE

The operating characteristics of the PEMWE are described through the relationships among electrolyzer current, cell voltage and hydrogen production [22]. The corresponding electrochemical relations are expressed as follows:

$$\begin{cases} n(t) = \frac{I(t)}{2F} \\ V_{\text{el}} = E_{\text{oc}} + V_{\text{act}} + V_{\text{con}} + V_{\text{ohm}} \end{cases} \tag{1}$$

where n represents the amount of substance of hydrogen produced (mol/s), I represents the electrolyzer current (A). And F is the Faraday constant (C/mol). V_{el} represents the voltage of the electrolyzer (V). While E_{oc}, V_{act}, V_{con} and V_{ohm} are the open-circuit voltage, activation polarization voltage, concentration difference polarization voltage and ohmic polarization voltage, respectively (V). The calculation formulas are as follows

$$\begin{cases} E_{\text{oc}} = E_0 + \frac{RT}{2F}[\ln(p_{\text{H}_2} p_{\text{O}_2}^{0.5})] \\ V_{\text{act}} = \frac{2RT}{F}[\text{arcsinh}(\frac{i}{2i_{0_\text{an}}}) + \text{arcsinh}(\frac{i}{2i_{0_\text{ca}}})] \\ V_{\text{con}} = -\frac{RT}{nF}\ln(1 - \frac{i}{i_{\max}}) \\ V_{\text{ohm}} = I \cdot R_{\text{ohm}} \end{cases} \tag{2}$$

where E_0 represents the reference voltage (V), R is the ideal gas constant ($\text{J}\cdot\text{mol}^{-1}\cdot\text{K}^{-1}$), T denotes the stack temperature (K), and p_{H_2} and p_{O_2} correspond to the hydrogen and oxygen pressures within the reaction chambers, respectively (Pa). The variable i indicates the current density (A/m^2), defined as $i = I/A$, where A is the cross-sectional area of the electrode (m^2). Additionally, i_{0_an} and i_{0_ca} denote the exchange current densities of the anode and cathode, respectively (A/m^2). $i_{\max}$ represents the maximum current density (A/m^2), and R_{ohm} is the equivalent ohmic resistance of cell (Ω).

To incorporate load-dependent conversion into the scheduling model, the specific-energy relation reported by Ferguson [22] is adopted. The coefficients correspond to a controlled plant temperature of 54 °C and an approximately 605 kW system, as given

in Equation (6.2) and Table 6.2 of that study. For the 200 kW case considered here, the relation is transferred at equal fractional load while retaining the corresponding specific energy. Its electrical boundary includes the upstream plant auxiliaries and hydrogen-storage compression represented in the source.

$$\begin{cases} f_t = \frac{P_{\mathrm{el},t}}{P_{\mathrm{el,r}}} \\ e_{\mathrm{H_2}}(f_t) = 16.18 f_t + 38.46 + \frac{4.26}{f_t} \end{cases} \tag{3}$$

$$m_{\mathrm{H_2},t} = \frac{P_{\mathrm{el,t}}}{e_{\mathrm{H_2}}(f_t)}, \quad f_t > 0 \tag{4}$$

In Equations (3) and (4), specific energy is expressed in kWh·kg^{-1}, hydrogen production rate in kg·h^{-1} and electrical power in kW. Hydrogen output is set to zero when the PEMWE is shut down. The fixed-temperature relation represents operation under temperature control; startup thermal transients remain outside the scheduling model.

2.2.2. The Haber–Bosch Ammonia Synthesis Unit

The Power-to-Ammonia (PtA) system comprises a hydrogen production unit via electrolyzer, an air separation unit (ASU), and an ammonia synthesis unit [23]. Given that the model for the electrolytic hydrogen production unit has been established previously, this section focuses on the modeling of the ammonia synthesis process utilizing the Haber–Bosch technique. The downstream auxiliary demand includes air separation, synthesis-loop cooling and synthesis-feed pre-compression. Hydrogen production electricity is accounted for separately. The part-load auxiliary model is adopted from Wang et al. [24] and expressed as follows:

$$P_{\mathrm{PtA}} = 0.64(0.2 q_{\mathrm{r}} u_t + 0.8 q_t) + 0.26 q_t \tag{5}$$

where q denotes the ammonia production rate (kg·h^{-1}), q_{r} represents its rated value, and u indicates the operating state. The HB-ASU specific electricity demand is 0.64 MWh·t^{-1}, of which 20% is assigned to a fixed on-state component. Synthesis-feed compression contributes a further 0.26 MWh·t^{-1} [24]. Since 1 MWh·t^{-1} equals 1 kWh·kg^{-1}, Equation (5) gives electrical power directly in kW. At the rated production rate of 20 kg·h^{-1}, the auxiliary power demand is 18 kW.

The fixed on-state component causes the specific auxiliary electricity demand to increase as ammonia production decreases, as expressed in Equation (6). This formulation represents part-load operation under regulated pressure and temperature conditions using the available process-level parameters. Detailed compressor and ASU efficiency maps are not introduced without component operating data. Furthermore, the auxiliary coefficients are varied by ±10% to examine their influence on scheduling. As total ammonia electricity demand also includes water electrolysis [25], the upstream PEMWE electricity is accounted for separately and is not added again to the PtA term.

$$e_{\mathrm{PtA}}(q) = 0.772 + 0.128 \frac{q_{\mathrm{r}}}{q_t}, \quad q > 0 \tag{6}$$

2.2.3. Battery Energy Storage System

The energy storage of a battery is represented by its state of charge (SOC), the calculation formula for which is presented as follows [26]

$$\begin{cases} E_{t+1} = E_t + (\eta_{\mathrm{ch}} P_{\mathrm{ch},t} - \frac{P_{\mathrm{dis},t}}{\eta_{\mathrm{dis}}}) \cdot \Delta t \\ SOC_t = \frac{E_t}{E_{\mathrm{r}}} \end{cases} \tag{7}$$

where E denotes the stored battery energy (kWh), and E_{r} is the rated capacity, set to 1600 kWh in the case study. Charging and discharging powers are expressed as nonnegative

values in kW. The charging and discharging efficiencies are each set to 90%, corresponding to an 81% round-trip efficiency. These values define the battery operating conditions adopted for the case study.

2.2.4. HST

HST receives hydrogen generated by the PEMWE while simultaneously supplying hydrogen to the ammonia synthesis unit. Accordingly, the capacity state of the storage tank can be calculated by the following formula:

$$H_{t+1} = H_t + (\dot{m}_{\mathrm{H}_{2,t}} - \frac{3}{17} q_t) \cdot \Delta t \tag{8}$$

where H denotes the hydrogen inventory (kg), $\dot{m}_{\mathrm{H}_{2,t}}$ represents the hydrogen production rate ($\mathrm{kg \cdot h^{-1}}$), q denotes the ammonia production rate ($\mathrm{kg \cdot h^{-1}}$), and Δt is the time interval (h). According to reaction stoichiometry, producing 1 kg of ammonia requires 3/17 kg of hydrogen. The tank is modeled as gaseous hydrogen storage, without a liquid–hydrogen boil-off term.

3. Multi-Objective Optimization Scheduling Model

The physical models characterize the mass and energy conversion relationships within each individual unit. Building upon the aforementioned models, a comprehensive optimization model for the system is established.

3.1. Day-Ahead Optimization Model

In designing the day-ahead scheduling plan, the economic efficiency and independent operational capability of the system are primarily considered. Specifically, this entails minimizing both the total operating cost and the frequency of power purchases from the main grid. The total operating cost of the system is calculated using the following equation: The operating-cost term additionally includes degradation costs for the PEMWE and BESS.

$$C_{total} = C_{purchase} - C_{sold} + C_{\mathrm{BESS}} + C_{\mathrm{PEM}} \tag{9}$$

where $C_{purchase}$ represents electricity purchase expenditure and C_{sold} denotes ammonia sales revenue. C_{BESS} and C_{PEM} represent the corresponding degradation costs. The case study permits electricity imports only, so no grid-export revenue is included. Electricity purchase expenditure and ammonia sales revenue are calculated as follows:

$$\begin{cases} C_{purchase} = \sum_{t=1}^{24} [Q_{purchase}(t) \cdot C_{\mathrm{ele},purchase}(t)] \\ C_{sold} = \sum_{t=1}^{24} [M_{sold}(t) \cdot C_{\mathrm{am},0}(t)] \end{cases} \tag{10}$$

where $Q(t)$ represents the quantity of electricity exchanged with the grid at time t (kWh), and $M_{sold}(t)$ denotes the mass of ammonia sold at time t (kg). $C_{\mathrm{ele},purchase}(t)$ indicates the unit price for purchasing electricity from the grid at time t (CNY/kWh), while $C_{\mathrm{am},0}(t)$ represents the unit price of ammonia at time t (CNY/kg). The degradation terms use battery internal energy throughput and PEMWE energized operating hours, as expressed below. Charging/discharging powers are in kW and the time interval is in h. t = 1, ..., 24 indexes the 24 hourly intervals of one day, with $\Delta t = 1$ h. The index $t = 0$ is reserved for the initial storage states and is excluded from interval-based cost and production summa-

tions. $Q_{purchase}(t)$ and $M_{sold}(t)$ are interval totals, so no addition-al Δt factor is required in Equation (10).

$$\begin{cases} C_{\mathrm{BESS}} = c_b \sum_{t=1}^{24} (\eta_{\mathrm{ch}} P_{\mathrm{ch},t} + \frac{P_{\mathrm{dis},t}}{\eta_{\mathrm{dis}}}) \cdot \Delta t \\ C_{\mathrm{PEM}} = c_h \sum_{t=1}^{24} u_{\mathrm{el},t} \cdot \Delta t \end{cases} \tag{11}$$

The battery replacement–value coefficient and cycle life are taken from [27]. The PEMWE stack cost and operating life are based on the DOE 2022-status values [28], with currency conversion according to [29]. The resulting cost coefficients are given below. These terms account for throughput-related and operating-hour-related wear. Calendar aging, cycle-depth dependence and additional damage from startup or thermal cycling require equipment-specific calibration and are not assigned separate monetary penalties here. In Equation (12), c_b is an energy-throughput cost coefficient (CNY/kWh), whereas c_h is the cost per energized operating hour of the 200 kW PEMWE stack (CNY/h).

$$\begin{cases} c_b = \frac{554}{2\times4000} = 0.06925 \text{ CNY/kWh} \\ c_h = \frac{450\times6.7168\times200}{40000} = 15.1128 \text{ CNY/h} \end{cases} \tag{12}$$

In summary, the multi-objective optimization problem for the day-ahead scheduling phase is formulated as follows:

$$f(x) = [C_{total}(x), N_{purchase}(x)] \tag{13}$$

where

$$x = (s_{\mathrm{el}}, s_{\mathrm{bat}}, s_{\mathrm{PtA}}, s_{\mathrm{G}}) \tag{14}$$

where s denotes the operational status of each device, as detailed in Table 1.

Table 1. Operational status of each device.

	−1	0	1
PEMWE (el)	-	Shutdown	Start
Battery (bat)	Discharging	Shutdown	Charging
Ammonia Synthesis Unit (PtA)	-	Shutdown	Start
Main Grid (G)	Buying electricity	-	-

3.2. Intra-Day Optimization Model

In the design of the intra-day dispatch plan, real-time operational performance must be considered subject to the constraints of the day-ahead scheduling framework. Specifically, this entails minimizing real-time operating costs and maximizing the renewable energy utilization rate. The real-time operating cost of the system is calculated as follows: The PEMWE and BESS degradation terms are included using the same accounting as the day-ahead stage. For full-day intra-day cost accounting, the corresponding sums run over k = 1, …, 96 with Δt = 0.25 h. Each implemented interval is counted once; overlapping rolling pre-diction horizons are not added together when reporting daily costs.

$$C_{operation} = C_{purchase} - C_{sold} + C_{\mathrm{BESS}} + C_{\mathrm{PEM}} \tag{15}$$

Similarly, the multi-objective optimization problem for the intra-day optimization phase is formulated as follows:

$$Minimize\ y = f(x) = [C_{operation}(x), Q_{purchase}(x)] \tag{16}$$

where

$$x = (P_{\mathrm{el}}, P_{\mathrm{ch}}, P_{\mathrm{dis}}, P_{\mathrm{PtA}}, P_{\mathrm{G}}) \tag{17}$$

where P represents the actual operating power of each device (kW).

3.3. Constraints

During system operation, the energy constraints can be expressed as follows:

$$P_{\mathrm{PV}}(t) + P_{\mathrm{dis}}(t) = P_{\mathrm{el}}(t) + P_{\mathrm{ch}}(t) + P_{\mathrm{PtA}}(t) + P_{\mathrm{Load}}(t) + P_{\mathrm{G}}(t) \tag{18}$$

$$n_{\mathrm{H_2,el}}(t) = \Delta n_{\mathrm{HST}}(t) + n_{\mathrm{PtA}}(t) \tag{19}$$

where $P_{\mathrm{PV}}(t)$ represents the power generation from renewable energy sources at time t (kW), and $P_{\mathrm{Load}}(t)$ denotes the power consumption of the electrical load at time t (kW). Additionally, $\Delta n_{\mathrm{HST}}(t)$ indicates the variation in the amount of hydrogen within the HST at time t (mol).

For the proposed system, the electrical power of each device is contingent upon its operational status. Consequently, the electrical power constraints for the devices are presented as follows:

$$\begin{cases} 0 \le P_{\mathrm{el}}(t) \le P_{\mathrm{el},rated} \\ 0 \le P_{\mathrm{ch}}(t), P_{\mathrm{dis}}(t) \le P_{\mathrm{bat},rated} \\ \alpha P_{\mathrm{PtA},rated} \le P_{\mathrm{H2A}}(t) \le P_{\mathrm{PtA},rated} \end{cases} \tag{20}$$

where P_{rated} denotes the rated power of each device (kW), and α represents the minimum maintenance coefficient of the ammonia synthesis unit. Constrained by the thermal equilibrium of the reactor and catalyst activity, this value is set to 20%.

To ensure operational safety and mitigate aging, upper and lower capacity limits are established for the energy storage units. Consequently, the capacity constraints for these devices are expressed as follows:

$$\begin{cases} E_{\min} \le E_t \le E_{\max} \\ H_{\min} \le H_t \le H_{\max} \end{cases} \tag{21}$$

where $E_{\min}$ and $E_{\max}$ represent the lower and upper capacity limits of the battery, respectively, while $H_{\min}$ and $H_{\max}$ denote the corresponding lower and upper limits for the HST (kg).

The core design philosophy of the aforementioned two-stage optimization model lies in decoupling the rapid dynamic responses of the power system from the slow process constraints of the chemical units, thereby achieving coordination across different time scales. In the day-ahead optimization phase, an hourly time step is utilized to formulate start-up and shutdown schedules for high-inertia equipment, such as the ammonia synthesis unit, with the primary objective of optimizing overall economic performance and system stability. Conversely, the intra-day optimization phase operates with a 15 min time step. Functioning within the framework established by the day-ahead schedule, this phase performs real-time power adjustments for fast-response devices, such as batteries and electrolyzers, to mitigate the transient fluctuations of renewable energy. Through this approach, the effective integration of decision-making processes across varying time scales is achieved.

4. Day-Ahead and Intra-Day Two-Stage Optimal Scheduling Strategy

4.1. Power Forecasting Algorithms

The proposed optimization framework incorporates power forecasting at two distinct temporal scales: day-ahead and intra-day. In the day-ahead phase, a Bidirectional Long Short-Term Memory network is employed to generate baseline predictions for unit commitment [26]. In the intra-day optimization phase, real-time forecasting for the subsequent time step is conducted based on historical meteorological data and preceding prediction values. This process necessitates an algorithm capable of effectively capturing the dynamic characteristics of power fluctuations. Therefore, a hybrid deep learning model integrating Convolutional Neural Networks (CNN) and Long Short-Term Memory (LSTM) networks is employed [27]. Furthermore, a rolling horizon forecasting mechanism is incorporated

to achieve multi-step look-ahead prediction. The fundamental architecture of this power forecasting algorithm is illustrated in Figure 2.

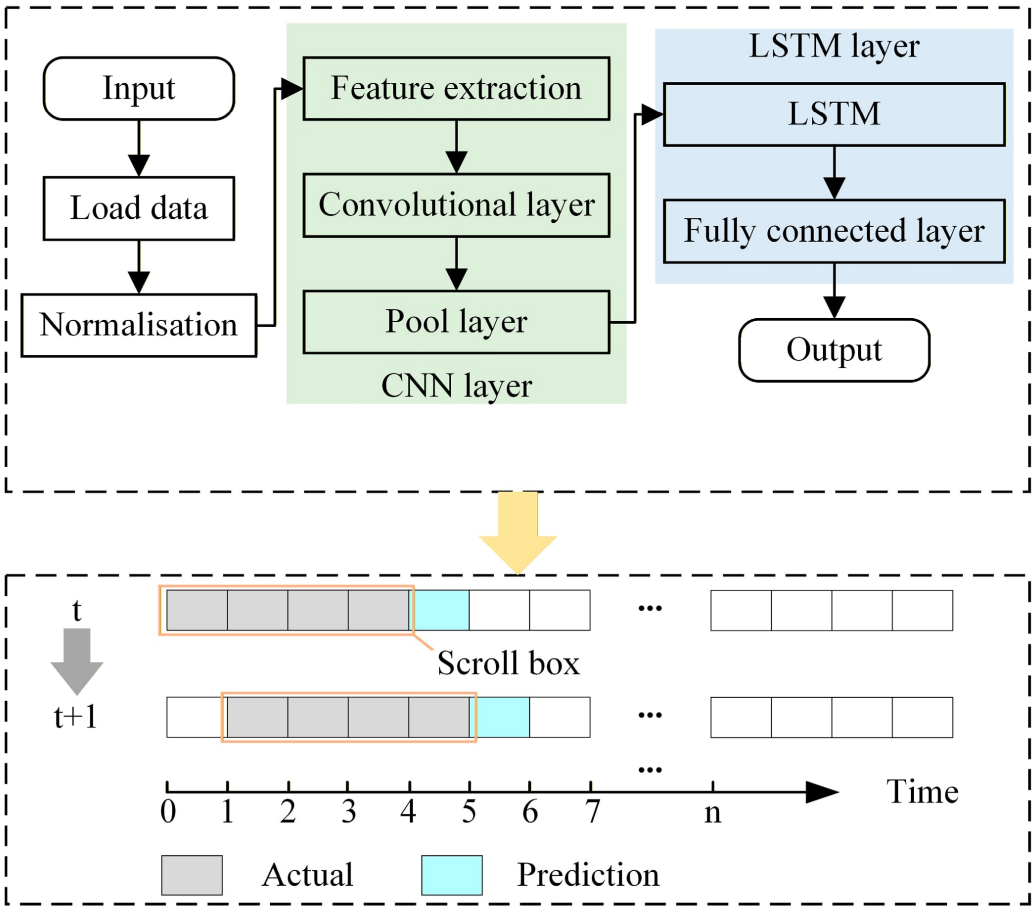


Figure 2. Flowchart of CNN-LSTM framework based on rolling horizon prediction.

In this study, in order to improve the prediction accuracy, historical data of different spans are selected for training and learning for day-ahead and intra-day prediction respectively. The parameter Settings of the prediction part are shown in Table 2.

Table 2. Parameter setting of power prediction model.

	Input Data Type	Data Time Span	Data Step Size
Day-ahead	Power data with time	7 days	1 h
Intra-day	Power data with time	2 days	15 min

4.2. Two-Stage Optimization Scheduling Model

In the constructed two-stage multi-objective optimization framework, at the day-ahead long time scale (hourly level), the model utilizes Mixed Integer Programming (MIP) to formulate high-level decisions regarding high-cost and slow-response processes based on day-long long-term forecasts of energy and load. Specifically, this involves determining the unit commitment status of critical equipment, such as the ammonia synthesis unit. These decisions establish rigid operational boundaries for the intra-day phase. Conversely, at the intra-day short time scale (15 min level), the focus shifts to strategy implementation. Strictly adhering to the start-stop constraints established in the day-ahead stage, the model employs dynamic optimization based on high-precision rolling forecasts to adjust the real-time operating power of each unit. This approach facilitates a rapid response to renewable energy

fluctuations and load uncertainties. This paradigm of 'day-ahead framework determination and intra-day precise adjustment' effectively resolves the conflict between the flexibility requirements of the power system and the stability demands of chemical production.

In summary, this study utilizes a power forecasting algorithm to obtain power data with time steps of 1 h and 15 min, respectively. The 1 h forecast data serves as the basis for the output scheduling of slow-response equipment (ammonia synthesis units) and the unit commitment of the remaining devices. Subsequently, the 15 min forecast outputs are utilized for the real-time rolling adjustment of device output power. By establishing indicators for both economic operation and independent stable operation, and integrating data from these two distinct time steps, the problem is solved and optimized using MIP. The specific flowchart is illustrated in Figure 3.

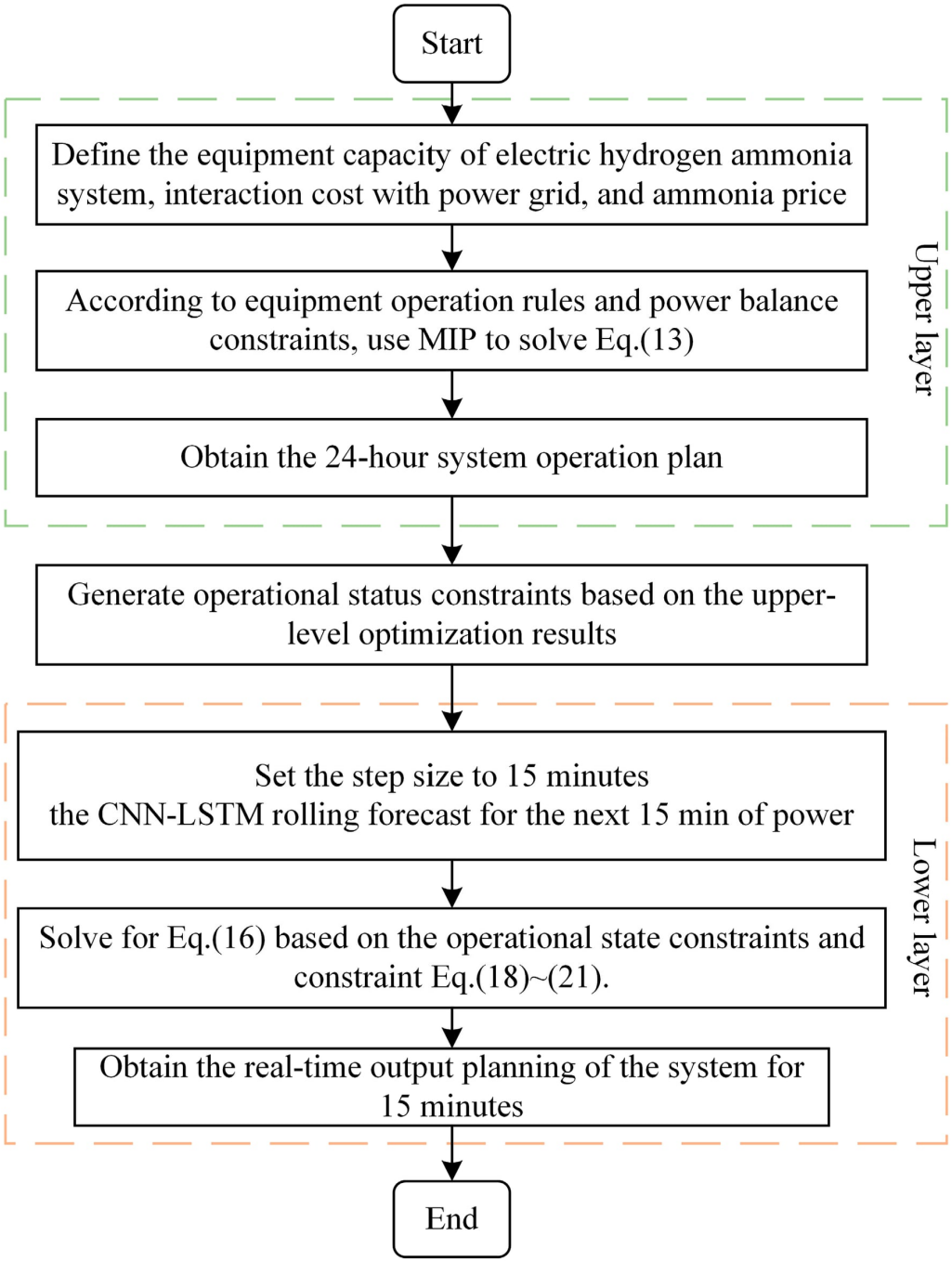


Figure 3. The process of model solving.

5. Results and Discussion

5.1. Case Study

The case study considers a 200 kW PEMWE, a 1600 kWh/400 kW BESS and a 500 kg HST. The rated ammonia production rate is 20 kg·h^{-1}, with a daily delivery requirement of 200 kg. At this production rate, Equation (5) gives an auxiliary electricity demand of 18 kW for the downstream ammonia section. The principal equipment capacities and operating limits are summarized in Table 3 as case-study design settings.

Table 3. System state parameters setting.

Parameter	Unit	Value
PV reference peak	kW	1500
HST capacity	kg	500
Battery capacity	kWh	1600
Rated power of PEMWE	kW	200
Minimum operating power of PEMWE	kW	20
Maximum ammonia production Rate	(kg/h)	20
Minimum ammonia production Rate	(kg/h)	4
Initial level of hydrogen storage	kg	250
Upper limit of hydrogen storage	kg	500
Lower limit of hydrogen storage	kg	20
Initial energy of battery	kWh	800
Upper limit of battery capacity	kWh	1280
Lower limit of battery capacity	kWh	320
PtA auxiliary power at rated production	kW	18

The electricity–hydrogen–ammonia production system is applicable to a wide range of building complexes and industrial parks, where the rated capacities of the equipment are primarily determined by local meteorological conditions and load profiles. Given that microgrid systems may face disconnection from the utility grid due to potential force majeure events, a certain degree of off-grid operational capability (islanding capability) is generally required in the design phase. Consequently, considering the capacity and rated power of the devices within the microgrid studied herein, the capability of the proposed system to operate in off-grid mode for 4 h will also be evaluated.

The load and PV profiles are obtained from the CoSSMic household channel DE_KN_residential3 in the Open Power System Data package [30]. Four local dates are selected to represent different seasonal conditions: 29 February, 1 May, 1 August and 1 November 2016. Each is the earliest complete day in its selected month without interpolation flags in the three required meter channels. Consumption is reconstructed from cumulative grid-import, PV-generation and grid-export readings. Forward differences over 0.25 h convert these energy measurements into average power. The resulting profiles are normalized to the case-study scale, providing a public-data basis for comparing the scheduling strategies under common economic inputs. The residential profile represents the baseline electrical demand of the microgrid and provides a measured time series for testing dispatch under varying demand. The electrical demand of hydrogen production and ammonia synthesis is modeled separately. At the same mean demand, a flatter industrial load profile could reduce the battery power required to cover short demand peaks. Its timing relative to PV generation could also change the electricity available to the PEMWE and thus the HST inventory.

As shown in Figure 4a–h, the 15 min load and PV profiles are compared with their corresponding hourly means. The four-day mean load of the selected source data is 0.7330833 kW, and the maximum PV output is 3.368 kW. To match the case-study design scale, the mean

load is normalized to 100 kW and the selected-day PV peak to 1500 kW. The corresponding transformations are expressed as follows:

$$\begin{cases} P_{x,t} = \frac{E_{x,t+1} - E_{x,t}}{0.25} \\ P_{L,t} = P_{\mathrm{imp},t} + P_{\mathrm{PV},t} - P_{\mathrm{exp},t} \\ P^{*}_{L,t} = \frac{100}{0.7330833333} P_{L,t} \\ P^{*}_{\mathrm{PV},t} = \frac{1500}{3.368} P_{\mathrm{PV},t} \end{cases} \tag{22}$$

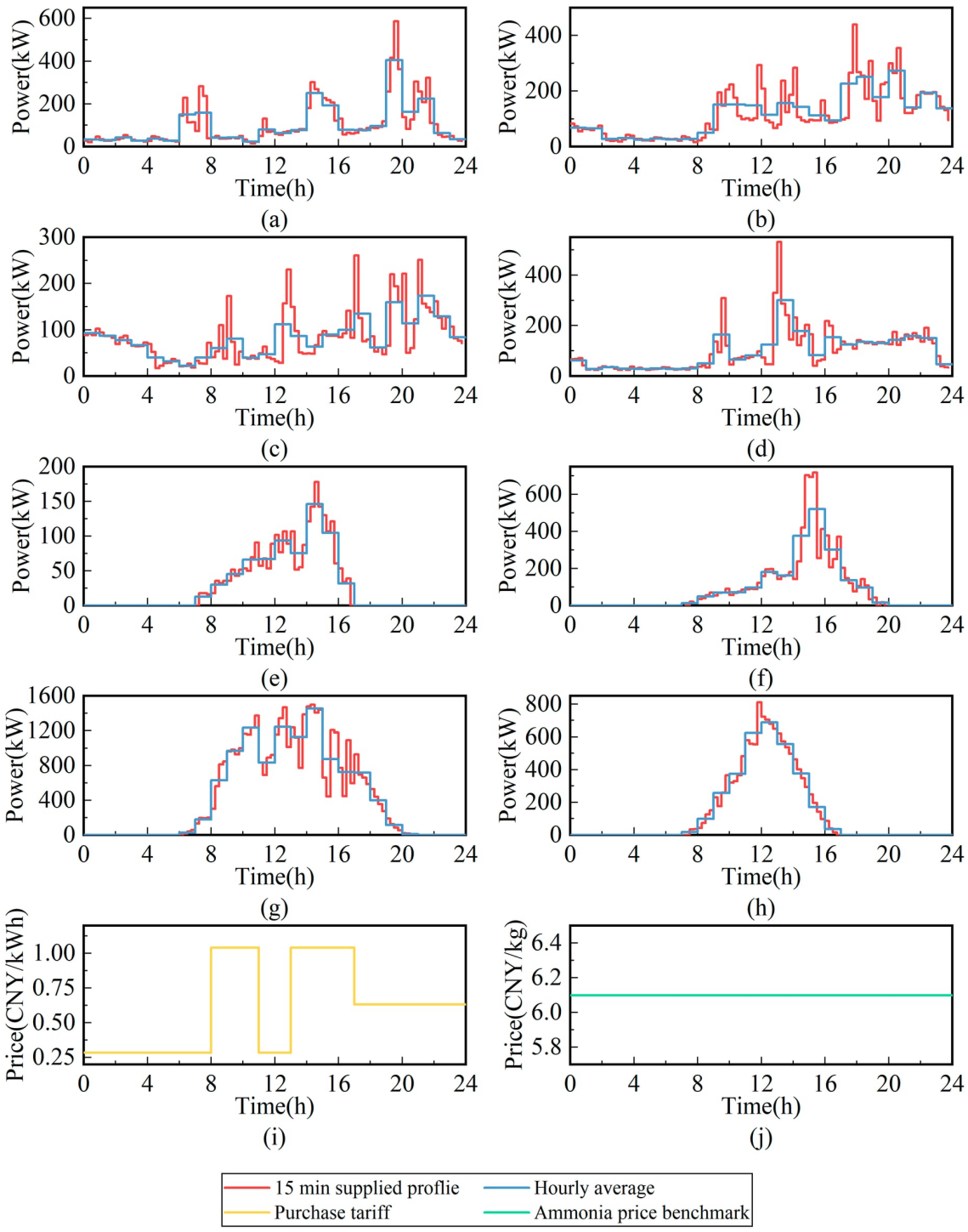


Figure 4. Input profiles and economic parameters. (**a**–**d**) Load profiles for Days 1–4. (**e**–**h**) Corresponding PV profiles. (**i**) Time-of-use electricity purchase tariff. (**j**) Ammonia-price benchmark.

For all grid-connected cases, the daily ammonia delivery requirement is imposed as follows:

$$\sum_{t=1}^{24} q_t \Delta t = 200 \text{ kg} \tag{23}$$

After normalization, the PV peaks for Days 1–4 are 178.15, 717.93, 1500.00 and 810.57 kW, respectively. The 1500 kW value therefore represents the selected profile reference peak, while the remaining days retain lower generation levels. Actual PV output depends on irradiance, temperature and operating losses, so it can differ from standard-test-condition nameplate power [31]. Since irradiance and module-area measurements are unavailable for these profiles, the normalization is not interpreted as a measurement of module conversion efficiency.

Figure 4i presents the time-of-use purchase tariff, with peak, flat and valley prices of 1.0417, 0.6313 and 0.2841 CNY·kWh^{-1}, respectively [32]. The peak periods are 08:00–11:00 and 13:00–17:00, the flat period is 17:00–24:00, and the valley periods are 00:00–08:00 and 11:00–13:00. The same historical tariff is applied to all four daily profiles, excluding holiday deep-valley pricing and demand/capacity charges. Figure 4j presents the ammonia-price input. The average net product price of EUR 811 ·t^{-1} is converted at CNY 7.5191 per EUR, giving a base price of CNY 6.0979901 ·kg^{-1} [29,33]. These common price inputs provide the basis for the operating-cost comparison.

5.2. On-Grid Model

Based on the power forecasting data obtained in the preceding section, the multi-objective optimization problem formulated in this study is solved. During grid-connected operation, electricity purchases supplement PV generation through the common electrical system. Both hydrogen production and ammonia auxiliary demand are included in the power balance. The numerical case enables imports only, while the physical interface remains bidirectional as shown in Figure 1.

In the following figures, PV generation, electrical loads and electricity purchases are represented by nonnegative magnitudes. For the BESS, positive net power denotes discharging and negative net power denotes charging. These conventions distinguish power generation from consumption without assigning negative values to PV production.

As shown in Figure 5, the grid-connected operating strategy coordinates electricity procurement with battery charging and discharging and electrolytic hydrogen production. Electricity purchases compensate for periods of insufficient PV output, while the storage devices connect energy supply and production demand across different intervals. The common daily delivery and terminal inventory requirements allow the four operating cases to be compared under the same economic conditions. If high variable costs of the kind observed on Days 1 and 2 recur, they would raise the operating cost component of the levelized cost of ammonia (LCOA). Recurring negative operating margins would reduce the cash flow available for capital recovery and could extend the payback period. Quantifying these effects requires representative annual operation and project investment and cash flow data.

The electricity purchases for Days 1–4 are 4113.93, 3104.46, 104.89 and 1527.32 kWh, respectively. After accounting for electricity expenditure and equipment degradation costs, the corresponding operating margins are −491.84, −169.81, 859.68 and 305.00 CNY/day. Day 3 combines the largest PV supply with the lowest grid electricity purchases and the highest operating margin. Conversely, the negative margins on Days 1 and 2 indicate that ammonia revenue does not cover the modeled variable costs under the fixed delivery obligation. Installation costs, financing and capital recovery remain outside this daily operating comparison.

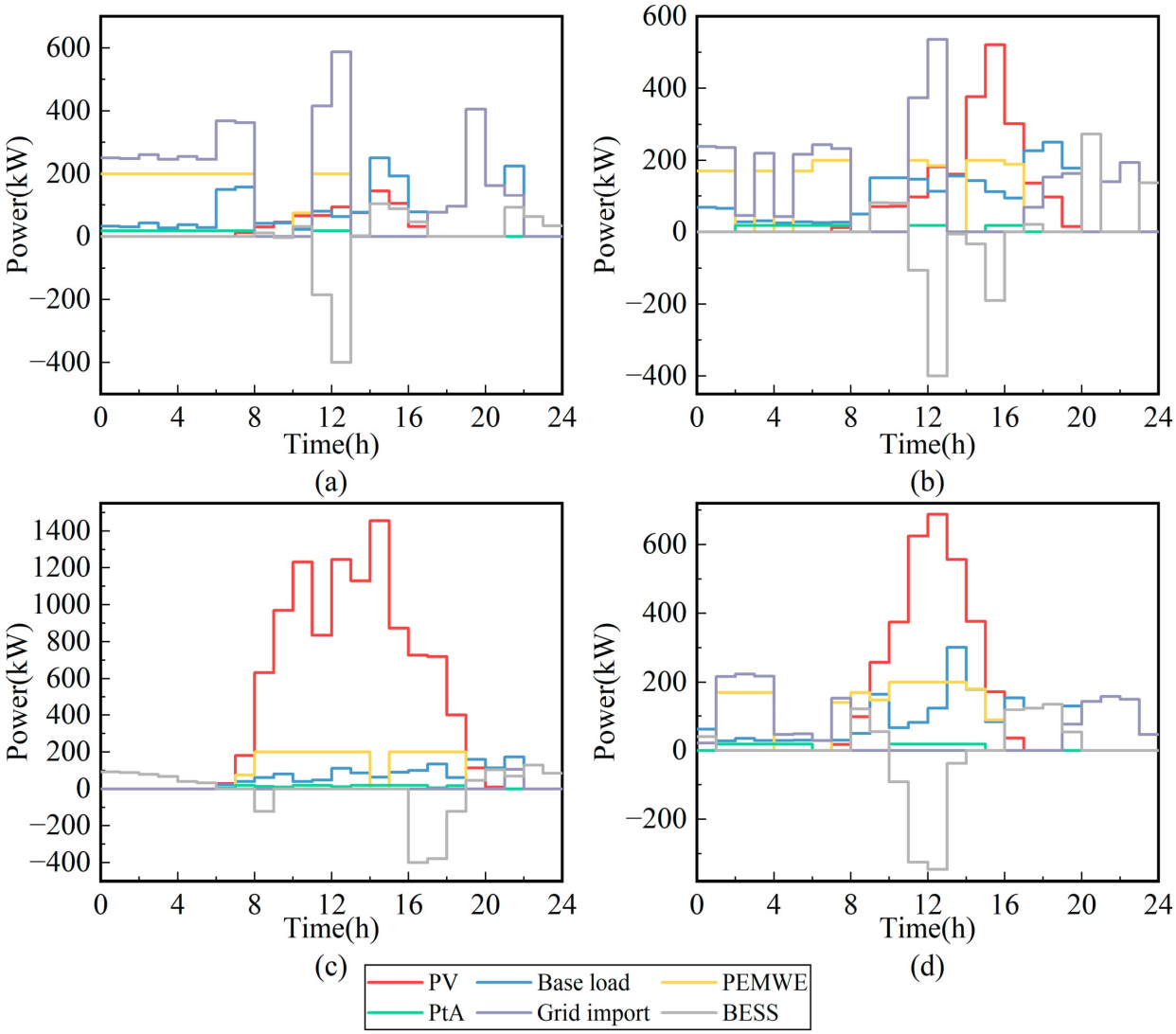


Figure 5. The output conditions of each unit (**a**–**d**) Day 1–4.

Throughout the scheduling horizon, battery energy and hydrogen inventory remain within their specified operating limits. Their end-of-day values are constrained to equal the initial values, so daily production is not supported by a net withdrawal of the initial storage reserves. Meanwhile, the HST permits the nonlinear hydrogen production rate to differ from the hourly ammonia feedstock demand.

When PV generation exceeds the combined consumption and charging capability, surplus electricity is curtailed because grid exports are disabled. The local PV utilization rates for Days 1–4 are 100.00%, 100.00%, 41.21% and 100.00%, respectively. Thus, the abundant generation on Day 3 reduces grid purchases but also produces substantial curtailment under the specified equipment capacities and export restriction.

As observed in Figure 6, SOC curve of the battery—representing a device with a faster response speed—exhibits significantly more pronounced fluctuations. In contrast, the LOH curve of the HST presents a much smoother profile. Operating on an hourly or even longer time scale, the hydrogen tank functions as a buffer for 'slow energy'—ammonia. It effectively decouples the hydrogen production rate of the electrolyzer from the hydrogen consumption demand of the ammonia synthesis unit, thereby guaranteeing the highly stable feedstock supply required by the downstream chemical process. This combination of 'fast electricity and slow hydrogen' constitutes the hybrid energy storage buffer chain emphasized in this

study. Through the conversion and coordination of different energy storage media, this optimization strategy successfully transforms drastic minute-level power fluctuations into stable, hour-level chemical production. This mechanism is identified as the key to achieving the efficient and stable operation of the electricity-chemical coupled system.

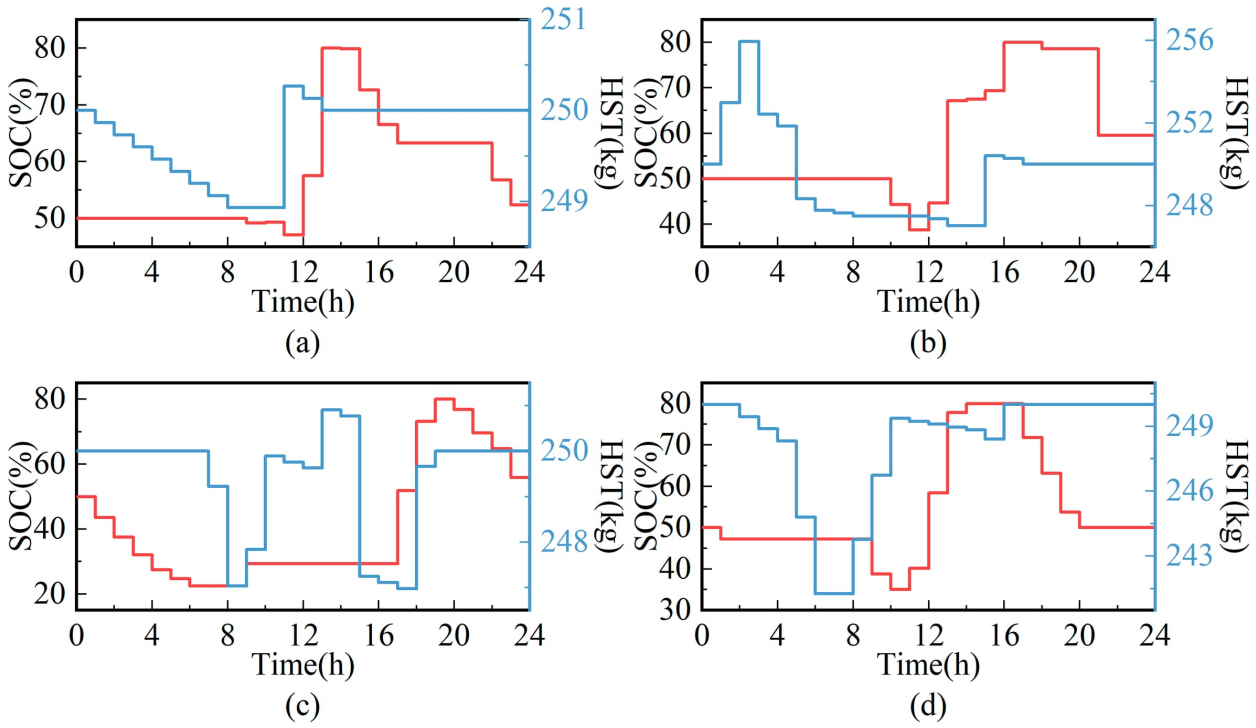


Figure 6. Energy storage level of energy storage device (**a**–**d**) Day 1–4.

The storage trajectories further reflect the different PV and load conditions on the four days. In each case, charging, discharging and hydrogen use are coordinated to satisfy the final inventory targets. These terminal conditions preserve the assumed reserve level for the following day. Different reserve requirements would alter the scheduling boundary and should therefore be considered when applying the framework to a specific installation.

As shown in Figure 7, ammonia production is arranged within the hourly operating intervals while satisfying the minimum operating-duration constraints. All four cases achieve a cumulative output of 200 kg, although the production periods differ with energy availability and electricity costs. The intra-day stage retains this chemical production plan and adjusts the PEMWE and BESS every 15 min. Through this arrangement, short-term electrical adjustment is carried out without repeatedly changing the hourly ammonia schedule. Larger CNN-LSTM forecast errors, as reflected in the mean absolute error (MAE) or root mean square error (RMSE), may increase intra-day operating costs. For example, overestimating PV output or underestimating load can require additional grid purchases or battery discharge during the 15 min adjustment, with the cost impact depending on the electricity tariff and available battery reserve.

In summary, the proposed multi-timescale two-stage optimization strategy effectively balances the multi-energy response characteristics across the electricity, hydrogen, and ammonia sectors, thereby ensuring the efficient and stable operation of the system under grid-connected conditions.

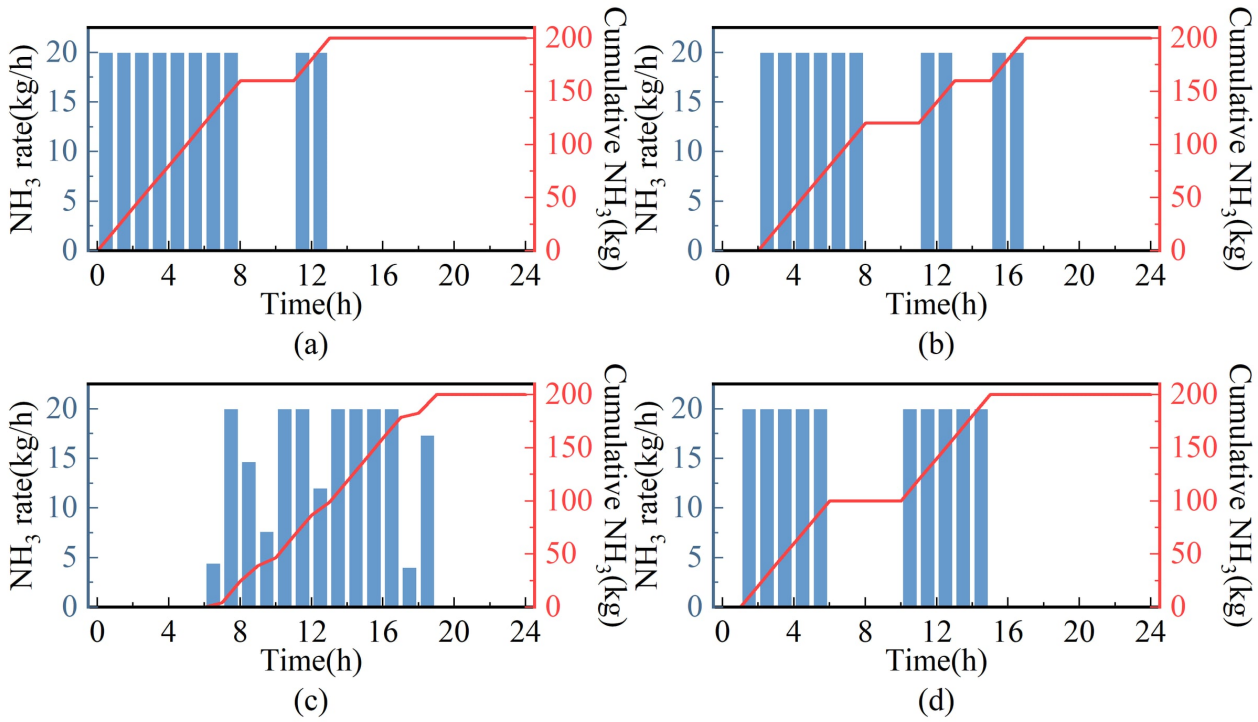


Figure 7. Ammonia production (**a**) Day 1; (**b**) Day 2; (**c**) Day 3; (**d**) Day 4.

5.3. Off-Grid Model

To examine short-term off-grid operation, three four-hour intervals are selected from Day 3: 00:00–04:00, 06:00–10:00 and 12:00–16:00. Each interval starts from the battery energy and hydrogen inventory obtained immediately before disconnection in the day-ahead schedule. Electricity exchange with the main grid is then set to zero. The permitted load-shedding fraction is varied from 0% to 40% in steps of 10%. First, the optimization minimizes unserved baseline electrical energy. Subsequently, it minimizes operating cost while maintaining the minimum unserved energy within numerical tolerance. This priority arrangement protects baseline electrical supply before discretionary chemical production. Accordingly, 40% represents the maximum permitted shedding in a test scenario rather than a prescribed shedding rate or a dynamic stability threshold.

As shown in Figure 8, PV generation is absent during 00:00–04:00, and the battery supplies the baseline electrical load and ammonia auxiliary demand. The PEMWE remains shut down, while the HST provides hydrogen to maintain ammonia synthesis. Over the four-hour interval, the system produces 80.000 kg of ammonia with 0.000 kWh of unserved baseline demand. The battery and hydrogen reserves therefore support off-grid operation throughout the tested low-light interval.

As shown in Figure 9, PV generation increases during 06:00–10:00 and progressively contributes to the electrical supply. The battery compensates for the initial power deficit, while stored hydrogen supplies the ammonia synthesis unit throughout the interval. Consequently, the PEMWE remains effectively shut down even as PV generation increases. Ammonia production reaches 80.000 kg, and the unserved baseline demand remains 0.000 kWh. This operating pattern illustrates how the inherited storage reserves separate short-term hydrogen production from chemical feedstock consumption.

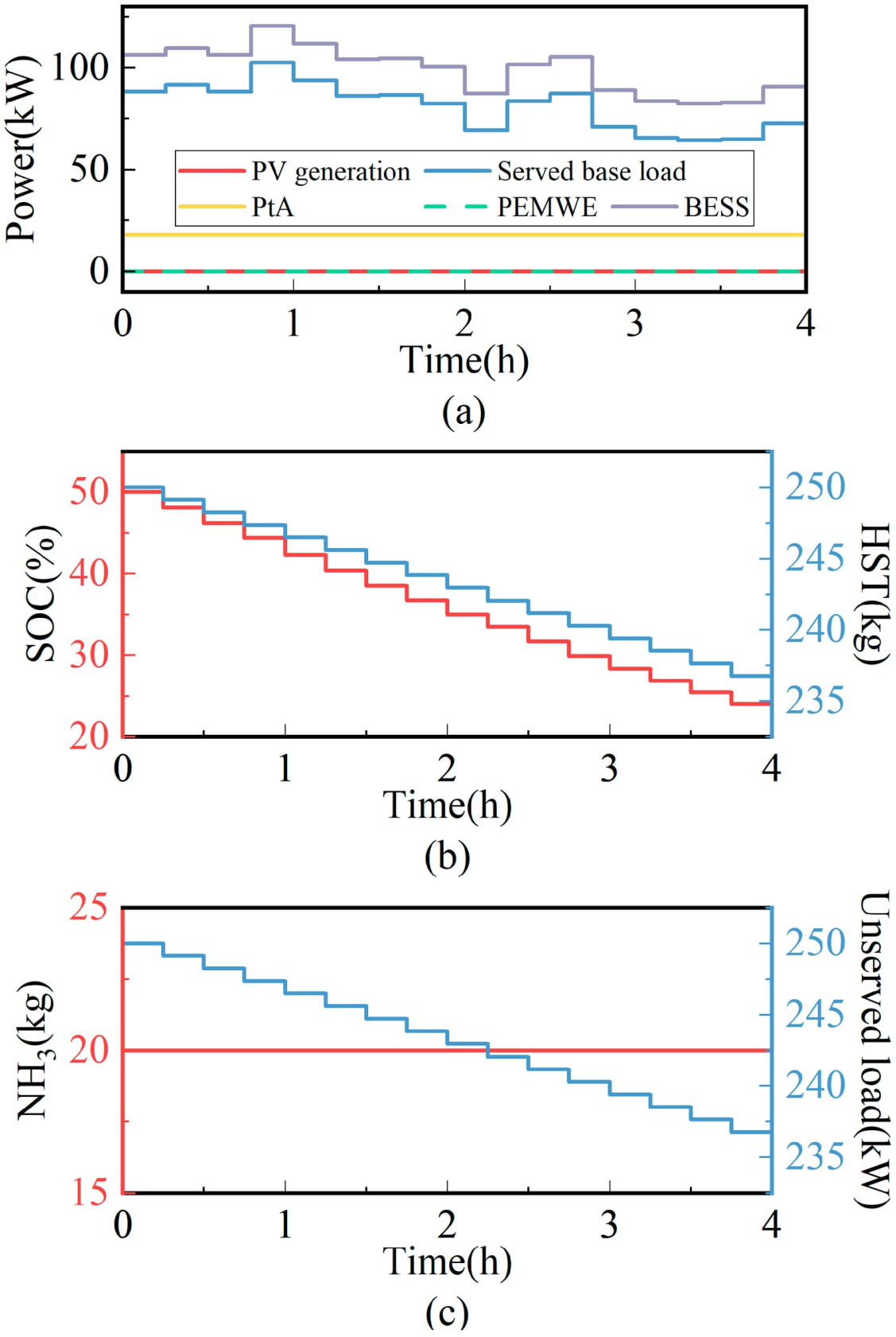


Figure 8. Four-hour off-grid operation during 00:00–04:00. (**a**) Operating power. (**b**) Battery SOC and HST inventory. (**c**) Ammonia production rate and unserved baseline load.

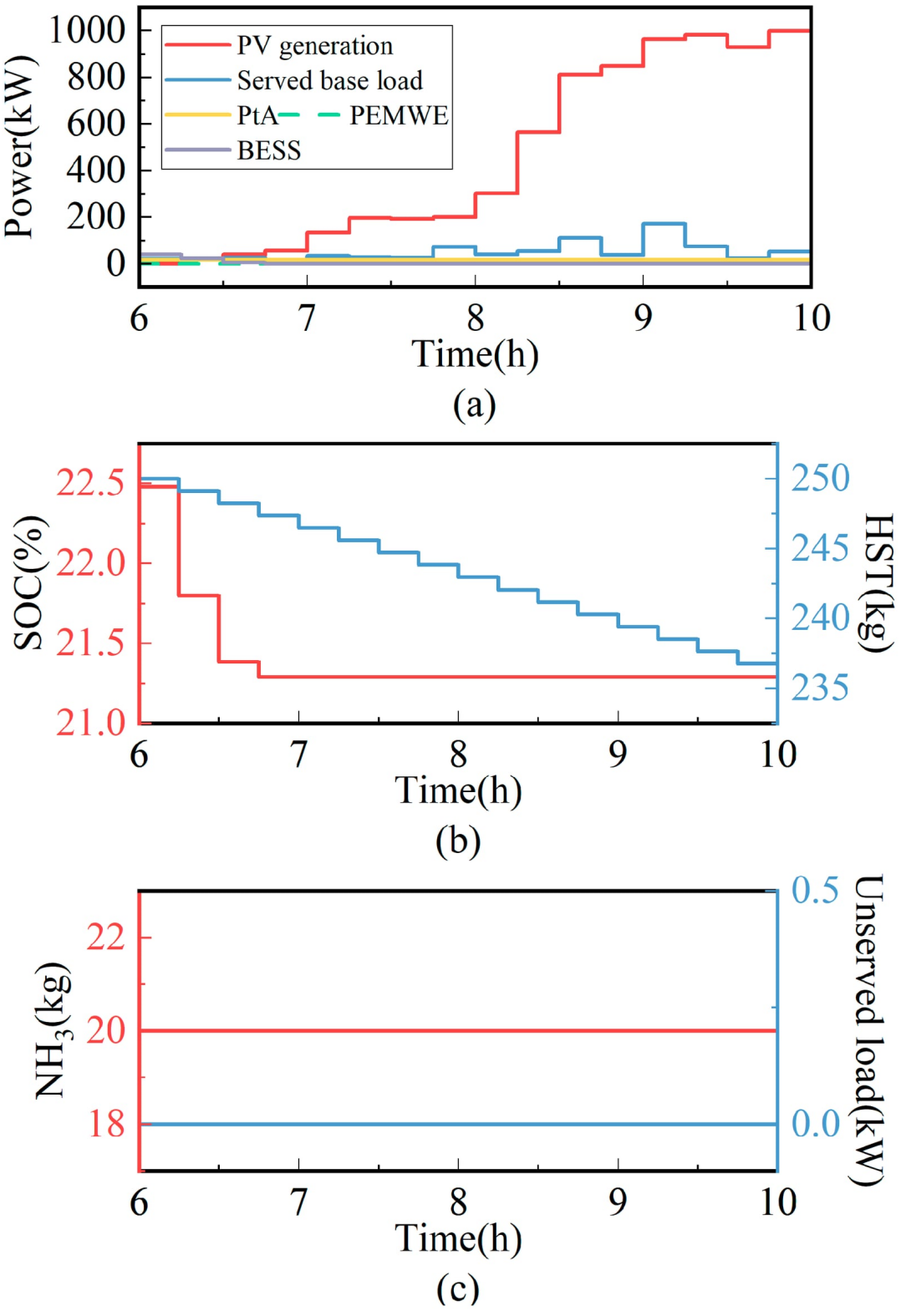


Figure 9. Four-hour off-grid operation during 06:00–10:00. (**a**) Operating power. (**b**) Battery SOC and HST inventory. (**c**) Ammonia production rate and unserved baseline load.

As shown in Figure 10, PV generation during 12:00–16:00 exceeds the electrical demand of the baseline load and ammonia auxiliaries. The schedule maintains the battery energy level and uses the HST inventory to support ammonia production, leaving the PEMWE shut down. Surplus PV generation is curtailed under the specified operating objective and export

restriction. The resulting ammonia output is 80.000 kg, with 0.000 kWh of unserved baseline demand. Thus, the short-term production requirement is satisfied without additional electrolysis or battery charging during this interval.

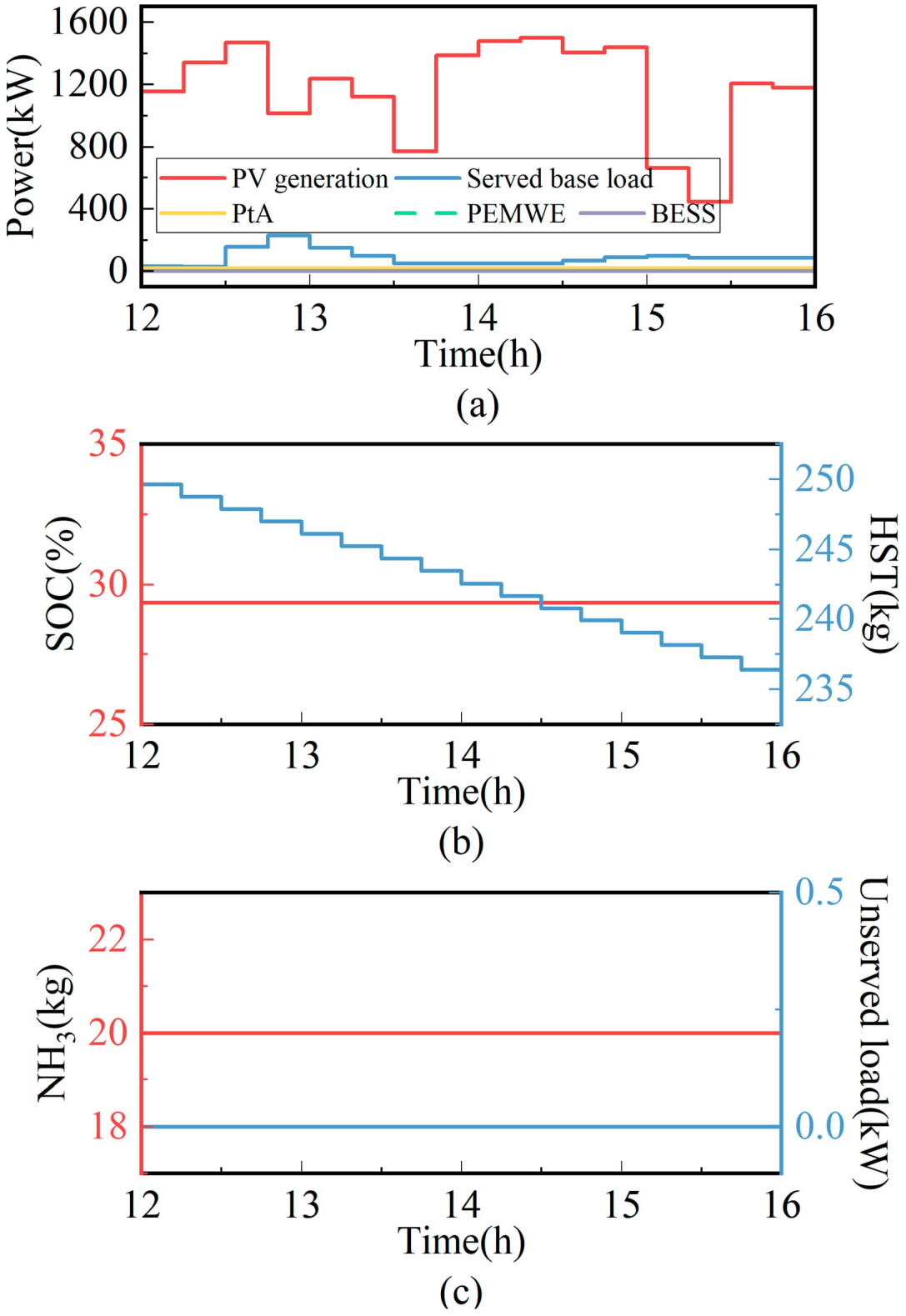


Figure 10. Four-hour off-grid operation during 12:00–16:00. (**a**) Operating power. (**b**) Battery SOC and HST inventory. (**c**) Ammonia production rate and unserved baseline load.

Furthermore, Figure 11b shows that all three off-grid windows remain feasible when the maximum shedding fraction is reduced to 0%. No baseline load shedding is therefore required within the tested range. This result depends on the available PV generation, inherited SOC and hydrogen reserves, rather than on a universal 40% criterion. For practical load prioritization, a feeder-level inventory is required to distinguish safety auxiliaries, instrumentation and essential services from interruptible production and discretionary demand. The present aggregate-load model evaluates scheduling feasibility; transient voltage and frequency behavior and safe chemical shutdown require separate dynamic assessment.

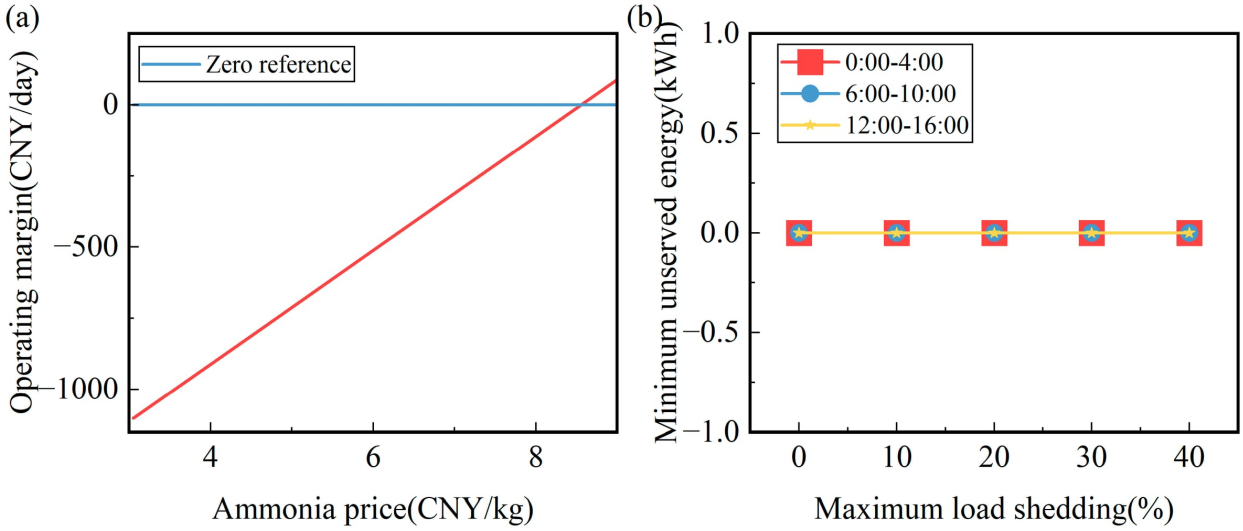


Figure 11. Sensitivity analysis. (**a**) Day 1 operating margin at different ammonia prices under a fixed daily delivery requirement. (**b**) Minimum unserved baseline energy for the three off-grid intervals at different maximum load-shedding fractions.

5.4. Sensitivity Analysis of Ammonia Price

To examine the influence of ammonia price on system economics, five price levels are considered at 50%, 75%, 100%, 125% and 150% of the base value. As shown in Figure 11a, the corresponding Day 1 operating margins are −1101.64, −796.74, −491.84, −186.94 and 117.96 CNY/day. The variable-cost break-even price is CNY 8.5572 ·kg^{-1}. Consequently, a higher ammonia price improves the daily operating margin, while the lower-price cases remain loss-making under the fixed production obligation.

Because the daily ammonia delivery is fixed at 200 kg, changing a constant daily sales price adds the same revenue increment to every feasible schedule. The operating margin therefore changes linearly with price, whereas the relative ranking of day-ahead production schedules remains unchanged, as expressed in Equation (24). This result identifies the role of the delivery constraint in the economic response. Price-responsive production would require a flexible-offtake arrangement or time-varying sales conditions. The price levels and ±10% auxiliary-consumption variations are deterministic sensitivity settings rather than measured market or equipment fluctuations.

$$\Pi(p) = 200p - C_{buy} - C_{\mathrm{BESS}} - C_{\mathrm{PEM}}, \quad \frac{d\Pi}{dp} = 200 \tag{24}$$

6. Conclusions

This paper investigates the multi-timescale collaborative optimization of an Integrated Electricity–Hydrogen–Ammonia Production System with hybrid energy storage. A coupled

energy and material flow model is established to represent nonlinear hydrogen conversion, ammonia auxiliary electricity consumption and battery–hydrogen storage coordination. Furthermore, an hourly day-ahead and 15 min intra-day scheduling framework is developed to account for the different operating time scales of electrical and chemical units. The main conclusions are summarized as follows:

(1) The coupled model describes the interactions among PEMWE conversion, battery energy, hydrogen inventory and ammonia production while accounting for equipment degradation costs. The case studies show that battery charging and discharging accommodate electrical variations, whereas hydrogen storage supplies ammonia feed-stock across different production intervals. This hybrid storage arrangement provides the scheduling buffer required to coordinate electrical operation with chemical production.

(2) The proposed day-ahead and intra-day framework satisfies the daily ammonia delivery requirement of 200 kg in all four grid-connected cases. The three four-hour off-grid cases also maintain ammonia production without baseline load shedding under the tested conditions. Meanwhile, ammonia-price sensitivity shows that the operating margin varies with product price, while the fixed delivery obligation leaves the relative ranking of feasible schedules unchanged. These results provide an operational reference for coordinated scheduling; equipment-specific degradation calibration, detailed critical-load priorities and transient process behavior remain topics for further study.

Author Contributions: Conceptualization, S.Z., J.Q. and K.S.; methodology, Z.C. and S.Z.; software, Z.C. and J.Z.; validation, F.F. and J.Z.; formal analysis, Z.C. and F.F.; investigation, Z.C. and J.Z.; resources, J.Q. and K.S.; data curation, Z.C. and F.F.; writing—original draft preparation, Z.C.; writing—review and editing, S.Z., J.Q., K.S. and F.F.; visualization, Z.C. and J.Z.; supervision, J.Q. and K.S.; project administration, J.Q. and K.S.; funding acquisition, J.Q. and K.S. All authors have read and agreed to the published version of the manuscript.

Funding: We acknowledge the support of the Shenzhen Energy Group Company Ltd. For the Key Technology Research Project of the Integrated Energy Utilization System of Photovoltaic Green Hydrogen.

Institutional Review Board Statement: Not applicable.

Informed Consent Statement: Not applicable.

Data Availability Statement: The original contributions presented in this study are included in the article. Further inquiries can be directed to the corresponding authors.

Conflicts of Interest: Authors Zhengjian Chen and Jingran Zhang were employed by the Shenzhen Energy Group Company Ltd. The authors declare that this study received funding from Shenzhen Energy Group Company Ltd. The funder was not involved in the study design, the data collection, analysis, or interpretation, the writing of this article, or the decision to submit it for publication. The remaining authors declare that the research was conducted in the absence of any commercial or financial relationships that could be construed as a potential conflict of interest.

References

1. Wu, B.; Wang, Z.; Tian, Y.; Zheng, S. The impact of industrial transformation and upgrading on fossil energy elasticity in China. *J. Clean. Prod.* **2024**, *434*, 140287. [CrossRef]
2. Zou, C.; Ma, F.; Pan, S.; Zhao, Q.; Fu, G.; Zhang, G.; Yang, Y.; Yu, H.; Liang, Y.; Lin, M.; et al. Global energy transition revolution and the connotation and pathway of the green and intelligent energy system. *Pet. Explor. Dev.* **2023**, *50*, 722–740. [CrossRef]
3. Xu, X.; Wang, B.; Shi, M.; Li, G.; Zhang, Y.; Wang, Q.; Liu, D. Research on hydrogen storage system configuration and optimization in regional integrated energy systems considering electric-gas-heat-hydrogen integrated demand response. *Int. J. Hydrogen Energy* **2025**, *135*, 86–103. [CrossRef]
4. Liang, T.; Zhang, X.; Tan, J.; Jing, Y.; Liangnian, L. Deep reinforcement learning-based optimal scheduling of integrated energy systems for electricity, heat, and hydrogen storage. *Electr. Power Syst. Res.* **2024**, *233*, 110480. [CrossRef]

5. Li, R.; Zhou, J.; Qiu, Z.; Li, H.; Li, J.; Wu, J.; Wu, K. Bi-level optimization of hybrid energy conversion system based on a multi-distinct low-carbon microgrid. *Renew. Energy* **2025**, *239*, 122095. [CrossRef]
6. Wang, J.; Mao, J.; Hao, R.; Li, S.; Bao, G. Multi-energy coupling analysis and optimal scheduling of regional integrated energy system. *Energy* **2022**, *254*, 124482. [CrossRef]
7. Liu, B.; Liu, Z.; Ren, J.; Xie, N.; Yang, S. Real-time operational optimization for flexible multi-energy complementary integrated energy systems. *J. Clean. Prod.* **2023**, *428*, 139415. [CrossRef]
8. Li, H.; Wei, Z.; Miao, Q.; Zhao, L.; Sun, B.; Zhang, C. Multi-energy flow cooperative dispatch for generation, storage, and demand in integrated energy systems with dynamic correction. *Sustain. Cities Soc.* **2022**, *76*, 103494. [CrossRef]
9. Zhang, N.; Sun, Q.; Yang, L. A two-stage multi-objective optimal scheduling in the integrated energy system with We-Energy modeling. *Energy* **2021**, *215*, 119121. [CrossRef]
10. Dias, E.X.; Bhavanari, M.; Lin, C.-H.; Aruna, P.T.; Tangirala, V.K.K.; Maddasani, S.; Tseng, C.-J. Advances in noble-metal-free electrocatalysts for alkaline seawater electrolysis: General mechanisms, challenges, and strategic innovations. *Renew. Energy* **2026**, *257*, 124798. [CrossRef]
11. Abdin, Z.; Khalilpour, K.; Catchpole, K. Projecting the levelized cost of large scale hydrogen storage for stationary applications. *Energy Convers. Manag.* **2022**, *270*, 116241. [CrossRef]
12. Ye, D.; Tsang, S.C.E. Prospects and challenges of green ammonia synthesis. *Nat. Synth.* **2023**, *2*, 612–623. [CrossRef]
13. Pagani, G.; Hajimolana, Y.; Acar, C. Green hydrogen for ammonia production–A case for the Netherlands. *Int. J. Hydrogen Energy* **2024**, *52*, 418–432. [CrossRef]
14. Armijo, J.; Philibert, C. Flexible production of green hydrogen and ammonia from variable solar and wind energy: Case study of Chile and Argentina. *Int. J. Hydrogen Energy* **2020**, *45*, 1541–1558. [CrossRef]
15. Müller, M.; Pfeifer, M.; Holtz, D.; Müller, K. Comparison of green ammonia and green hydrogen pathways in terms of energy efficiency. *Fuel* **2024**, *357*, 129843. [CrossRef]
16. Karimi, S.; Kwon, S. Optimization-driven uncertainty forecasting: Application to day-ahead commitment with renewable energy resources. *Appl. Energy* **2022**, *326*, 119929. [CrossRef]
17. Shen, F.; Cao, Y.; Shahidehpour, M.; Xu, X.; Wang, C.; Wang, J.; Zhai, S. Predict-and-Optimize Model for Day-Ahead Inertia Prediction Using Distributionally Robust Unit Commitment With Renewable Energy Sources. *IEEE Trans. Power Syst.* **2025**, *40*, 2688–2699. [CrossRef]
18. Shen, W.; Zeng, B.; Zeng, M. Multi-timescale rolling optimization dispatch method for integrated energy system with hybrid energy storage system. *Energy* **2023**, *283*, 129006. [CrossRef]
19. Yang, Z.; Zheng, X.; Sun, S.; Gao, C.; Guo, P.; Ding, X.; Sun, W. Collaborative optimization of hydrogen energy storage-aided multi-energy complementary systems: Resilience weight regulation and hybrid storage planning. *Energy Convers. Manag.* **2026**, *348*, 120768. [CrossRef]
20. Ma, T.; Li, M.-J.; Fan, C.-H.; Dong, H.-S. A novel real-time dynamic performance evaluation and capacity configuration optimization method of generation-storage-load for integrated energy system. *Appl. Energy* **2024**, *374*, 123896. [CrossRef]
21. EPEX SPOT. Basics of the Power Market. Available online: https://www.epexspot.com/en/basicspowermarket (accessed on 7 November 2026).
22. Ferguson, J.L.B. Technoeconomic Modelling of Renewable Hydrogen Supply Chains on Islands with Constrained Grids. Ph.D. Thesis, University of Edinburgh, Edinburgh, UK, 2021. Available online: https://era.ed.ac.uk/bitstream/handle/1842/37920/FergusonJ_2021.pdf?sequence=1 (accessed on 7 November 2026).
23. Zhang, W.; Zhang, M.; Liu, J. Optimal multi-energy storage capacity allocation for electricity-heat-hydrogen-ammonia integrated energy systems with ammonia cycling. *Renew. Energy* **2026**, *257*, 124788. [CrossRef]
24. Wang, C.; Walsh, S.D.C.; Longden, T.; Palmer, G.; Lutalo, I.; Dargaville, R. Optimising renewable generation configurations of off-grid green ammonia production systems considering Haber-Bosch flexibility. *Energy Convers. Manag.* **2023**, *280*, 116790. [CrossRef]
25. Schmidt, A.; Köster, D.; Strube, J. Climate Neutrality Concepts for the German Chemical–Pharmaceutical Industry. *Processes* **2022**, *10*, 467. [CrossRef]
26. Zhu, S.; Du, B.; Lu, X.; Xie, C.; Li, Y.; Huang, Y.; Zhang, L.; Zhao, B. Design and optimization of a cascade hydrogen storage system for integrated energy utilization. *J. Energy Storage* **2024**, *96*, 112732. [CrossRef]
27. Zhang, L.; He, Y.; Ma, Y.; Huang, C.; E, J. Degradation-Aware Deep Reinforcement Learning for Battery Energy Storage Dispatch in Industrial Microgrids and Its Real-Time Deployment Validation. *Energies* **2026**, *19*, 4997. [CrossRef]
28. U.S. Department of Energy. Technical Targets for Proton Exchange Membrane Electrolysis. Available online: https://www.energy.gov/cmei/fuels/technical-targets-proton-exchange-membrane-electrolysis (accessed on 7 November 2026).
29. China Foreign Exchange Trade System. RMB Central Parity Rates. 6 November 2026. Available online: https://www.chinamoney.com.cn/chinese/bkccpr/ (accessed on 7 November 2026).

30. Open Power System Data. Data Package Household Data, Version 2020-04-15. Available online: https://data.open-power-system-data.org/household_data/2020-04-15/ (accessed on 7 November 2026).
31. Sandia National Laboratories. PVWatts. PV Performance Modeling Collaborative. Available online: https://pvpmc.sandia.gov/modeling-guide/2-dc-module-iv/point-value-models/pvwatts/ (accessed on 7 November 2026).
32. State Grid Zhejiang Electric Power Co., Ltd. Announcement of Electricity Purchase Prices for Industrial and Commercial Users, October 2025. Available online: https://zjjcmspublic.oss-cn-hangzhou-zwynet-d01-a.internet.cloud.zj.gov.cn/jcms_files/jcms1/web3235/site/attach/0/c930701af7754b48b43ebd9359ef2a62.pdf (accessed on 7 November 2026).
33. Hintco. Lot 1 Renewable Ammonia. Available online: https://hintco.eu/lot-1-renewable-ammonia/ (accessed on 7 November 2026).

Disclaimer/Publisher's Note: The statements, opinions and data contained in all publications are solely those of the individual author(s) and contributor(s) and not of MDPI and/or the editor(s). MDPI and/or the editor(s) disclaim responsibility for any injury to people or property resulting from any ideas, methods, instructions or products referred to in the content.